Journal of Power Sources 270 (2014) 386–390

Contents lists available at ScienceDirect

Journal of Power Sources

journal homepage: www.elsevier.com/locate/jpowsour

Short communication

Ruthenium oxide modified titanium dioxide nanotube arrays as carbon and binder free lithium–air battery cathode catalyst

Guangyu Zhao, Yanning Niu, Li Zhang, Kening Sun*

Academy of Fundamental and Interdisciplinary Sciences, Harbin Institute of Technology, Harbin, Heilongjiang 150080, PR China

HIGHLIGHTS

- Carbon and binder free Li–O_2 battery cathodes constructed by a bottom-up method.
- RuO_2 catalyst on a stable TiO_2 nanotube array catalyst support.
- More than 100 cycle charge/discharge.

ARTICLE INFO

Article history:
Received 14 April 2014
Received in revised form
12 June 2014
Accepted 17 July 2014
Available online 24 July 2014

Keywords:
Lithium–air battery
Cathode
Carbon and binder free
Ruthenium oxide catalyst
Titanium dioxide nanotube array

ABSTRACT

RuO_2 modified TiO_2 nanotube arrays, growing on Ti foams, are used as carbon and binder free cathodes for Li–O_2 batteries. The micrometer pores in Ti foams and nanometer pores in TiO_2 nanotubes supply facilitated transport channels for oxygen diffusing into/out of the catalysts in discharge and charge processes. The RuO_2 catalyst exhibits outstanding catalytic active toward oxygen evolution reaction (OER), which leads the charge voltage maintaining around 3.7 V all through the battery cycling. The stability of TiO_2/Ti support, abundant oxygen transport path and favorable catalytic activity of RuO_2 toward OER enable the Li–O_2 batteries exhibiting 130 cycle discharge/charge.

1. Introduction

RuO_2 has attracted great interest as cathode catalyst for Li–air batteries by its favorable electron conductivity and good catalytic activity towards oxygen evolution reaction (OER). Various carbon materials, such as reduced graphene [1], carbon black [2] and carbon nanotubes [3,4] supported RuO_2 were implemented as oxygen cathodes of Li–air batteries, which exhibited high round-trip efficiency and outstanding catalytic ability. The most attractive characteristic is the low charge voltages of these batteries, about 3.7 V vs. Li^+/Li, much lower than those catalyzed by carbon materials only. The low charge voltage should be attributed to the strong catalytic ability of RuO_2 to OER. Ryung Byon and his coworkers [4] suggested that, RuO_2 contribute to the formation of poorly crystalline Li_2O_2 coated over the catalyst with large contact area during oxygen reduction reaction. Then this unique Li_2O_2 structure could be smoothly decomposed at low potential upon OER by avoiding the energy loss associated with the decomposition of the more typical Li_2O_2 structure with a large size, small contact area, and insulating crystals. However, all the studies mentioned above still used carbon materials as catalyst support and implemented conventional air cathode preparation approach, that mixing catalysts with conductive carbons and organic binders then pasting on the porous metal current collectors. Unfortunately, both carbon materials and organic binders have been reported degrading in Li–air batteries [5–11], which causes the instability of Li–air batteries' cathodes, harming batteries' rechargeability. Accordingly, the exploration of carbon and binder free cathodes is urgent for Li–air batteries [12–14].

TiO_2 is an attractive support material for catalyst, because it is stable, environmentally friendly and biocompatible [15–19]. Recently, Bruce and his co-workers [20] reported that, the stability of the TiO_2-rich surface layer present on the Li–air batteries' cathodes is responsible for the stable and reversible Li_2O_2 formation/decomposition. Therefore, TiO_2 is a good candidate for catalyst

* Corresponding author. Tel./fax: +86 451 86412153.
E-mail addresses: zhaogy810525@gmail.com (G. Zhao), keningsunhit@126.com (K. Sun).

http://dx.doi.org/10.1016/j.jpowsour.2014.07.112
0378-7753/

support of Li–air battery cathode. In various TiO_2 materials, nanotubes have drawn considerable attention, because of their large specific surface area and abundant mass transport channels. [21] The large surface area can supply abundant sites to accommodate Li_2O_2 precipitate. Moreover, the straight channels in the nanotubes are beneficial for oxygen transport, enhancing rechargeability and cyclability of Li–air batteries. [22] In present study, we fabricate TiO_2 nanotube arrays on Ti foams, and use the foams as substrates for Li–O_2 battery cathodes. Then RuO_2 catalyst is deposited on TiO_2 support directly by electrodeposition, avoiding using any organic binder. The RuO_2/TiO_2 cathodes exhibit good catalytic activity towards OER and enable the batteries exhibiting outstanding cycle performances.

2. Experimental

2.1. Sample preparation

The TiO_2 nanotube arrays were fabricated directly on circular titanium foam plates (thickness 0.5 mm, diameter 15 mm, 99.2% purity) using anodic oxidation. The Ti plates were initially sonicated in acetone, rinsed with pure water, and then etched in 5% HF for 2 min to remove any oxides from the surface. The etched Ti plate was then submerged in a two-electrode cell containing dimethyl sulfoxide (DMSO) + 2 wt% HF and was electrochemically treated via anodization at 20 V for 3 h. The as-anodized plates were washed with deionized water for depositing RuO_2. RuO_2 was deposited on anodized Ti foams by electrodeposition, which was carried out by cyclic voltammogram (CV) in a potential window of −0.8–2.0 V (vs. SCE) with a scan rate of 50 mV s^{-1} using a CHI 660 electrochemical analyzer. The anodized Ti foams were used as working electrode, a 1 cm × 1 cm Pt plate electrode was used as counter electrode, and SCE was used as reference electrode. The electrolyte for electrodeposition was consisted of 10 mM $RuCl_3$ and 1.2 mM HCl. In the CV process, Ru^{3+} ions were reduced to metal Ru on the anodized Ti foams in cathodic process, and the Ru metal was oxidized to RuO_2 in the subsequent anodic process [23]. The generated RuO_2 could not be reduced in the following cathodic process. Therefore, the sweeping caused the RuO_2 growing on the anodized Ti foams [24]. The as-deposited plates were washed, dried and annealed in an oven at 650 °C for 3 h. The weights of the deposited product were measured on a micro-balance (Mettler Toledo) with an accuracy of 0.01 mg. The RuO_2 loading amount on a plate was about 0.1 mg. The RuO_2 modified TiO_2 nanotube array coated Ti foams in this study is abbreviated as “RTT” in the following text.

2.2. Instruments for characterization

Scanning electron microscope (SEM) images were obtained on a Hitachi Su-8100. The X-ray diffraction (XRD) patterns were obtained on a PANalytical X'pert PRO X-ray diffractometer with Cu Kα radiation (λ = 1.5418 Å). X-ray photoelectron spectra (XPS) were obtained with a K-Alpha electron spectrometer (Thermofish Scientific Company) using Al Kα (1486.6 eV) radiation. The base pressure was about 1 × 10^{-8} mbar. The binding energies were referenced to the C1s line at 284.8 eV from adventitious carbon.

2.3. Li–O_2 battery tests

The Swagelok type Li–O_2 batteries were assembled inside an MBraun glove box. The cells were constructed by placing a 15 mm diameter Li disk on the bottom, covering it with a piece of glass fiber separator (20 mm diameter, Whatman), adding excessive electrolyte (1.0 M LiTFSI in tetraethylene glycol dimethyl ether (TEGDME)), placing an air electrode disk on the separator, and sealing the Swagelok cell. All the electrochemical measurements on the batteries were carried out in pure O_2 at 1 atm (99.99%). A BTS-2000 Neware Battery Testing System was employed for charge/discharge tests. For comparison, electrochemical measurements of super P carbon material were also studied as the Li–O_2 battery cathode catalyst. The battery assembling process was consistent with above, except the cathodes were prepared with a conventional carbon based air cathode preparation method. The details are mixing super P with the solution (10 wt%) of Polyvinylidene Fluoride (PVDF) containing N-methyl-2-pyrrolidone (NMP) in a weight ratio of carbon: PVDF = 4: 6, pasting the obtained homogeneous mixture on circular Cu foam plates (with diameter of 15 mm and thickness of 0.5 mm), drying the plates in a vacuum oven for 24 h on 120 °C. The dry plates were applied as the cathodes of Li–O_2 batteries.

3. Results and discussion

The SEM images of pristine Ti foams are shown in Fig. 1. The Ti foams are fabricated by hot briquetting from small Ti sands, and commonly used as the filtration devices for air/water treatment. The interspace between the Ti sands endows the Ti foams good gas/liquid permeability, which causes it attractive current collector for Li–O_2 batteries. Certainly, the outstanding stability of Ti metal compared with Al, Fe, Cu, Ni and the other common current collectors is another reason, that we choose it as the cathode substrate [25]. The SEM images of anodized Ti foams are shown in Fig. 2. Fig. 2(a) and (b) are the vertical views of the TiO_2 nanotube arrays, which demonstrate close packing of TiO_2 nanotubes, free-standing on the Ti substrates. The tube diameter is about 150 nm, and the tube wall is about 20 nm, as seen in Fig. 2(a). The bottom views of the films in Fig. 2(c) and (d) also exhibit close packing morphology of the nanotubes. Fig. 3(a) and (b) are the SEM images of the nanotube arrays deposited with RuO_2, demonstrating the nanoparticle morphology with several decade nanometers on the tube

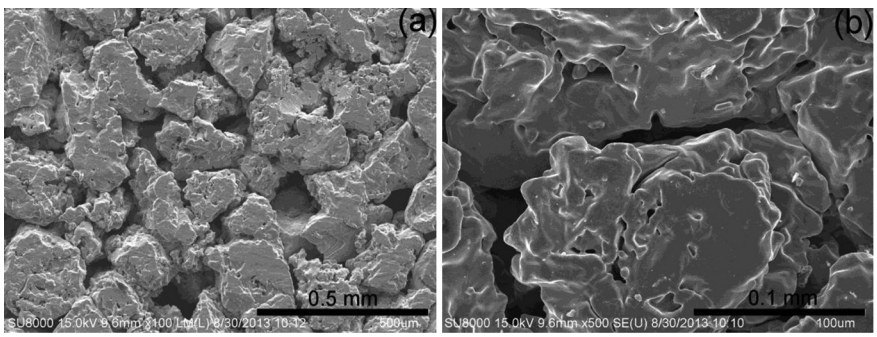

Fig. 1. SEM images of Ti foams.

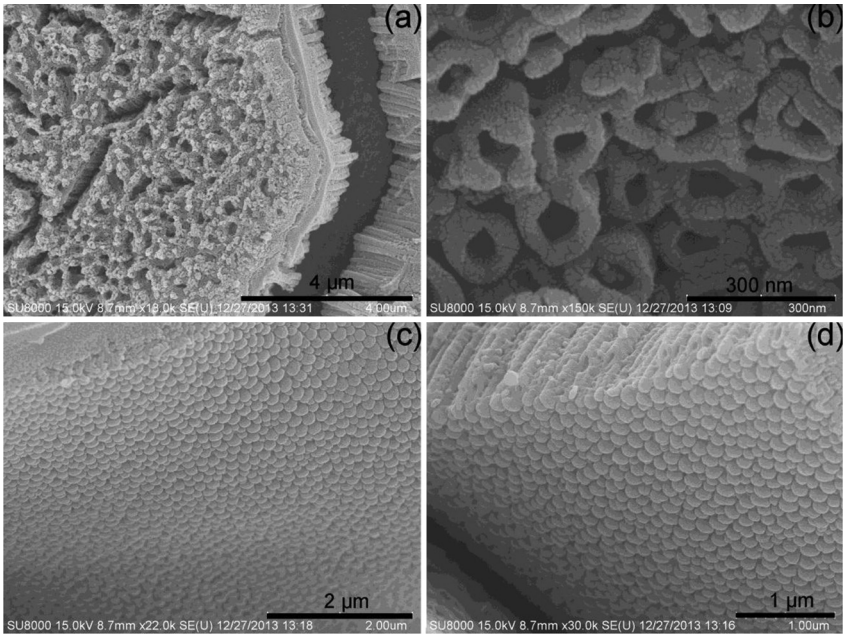

Fig. 2. SEM images of TiO_2 nanotube arrays: (a, b) vertical views; (c, d) bottom views.

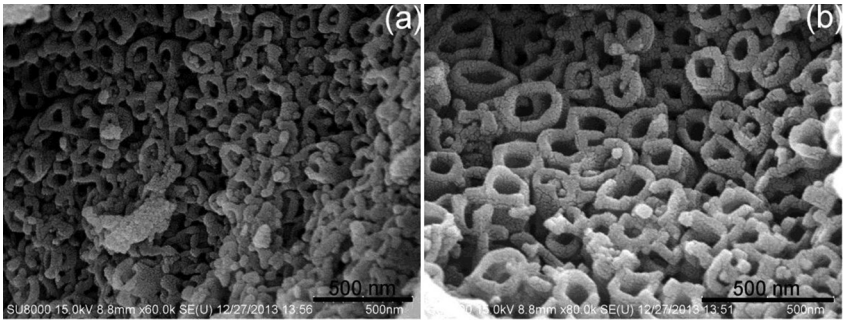

Fig. 3. SEM images of the as-prepared RuO_2 modified TiO_2 nanotube arrays electrodes.

walls. The XRD pattern of the RTT in Fig. 4 illustrates that, the TiO_2 is an anatase (JCPDS: 21-1272) and rutile (JCPDS: 21-1276) hybrid crystal form, resulted from the high sinter temperature. Although the 650 °C sinter temperature can ensure RuO_2 generating, its small amount compared with Ti and TiO_2 causes its peaks not detective in the XRD pattern. However, the XPS results reveal the existence of RuO_2 on the electrode surface unambiguously. Fig. 5(a) and (b) are the high resolution patterns of Ti 2p and Ru 3d of the as-prepared plates, respectively. The Ti 2p peak can be assigned to TiO_2 (Binding energy = 458.7 eV), and the Ru 3d peak can be assigned to RuO_2 (Binding energy = 281.5 eV) primarily.

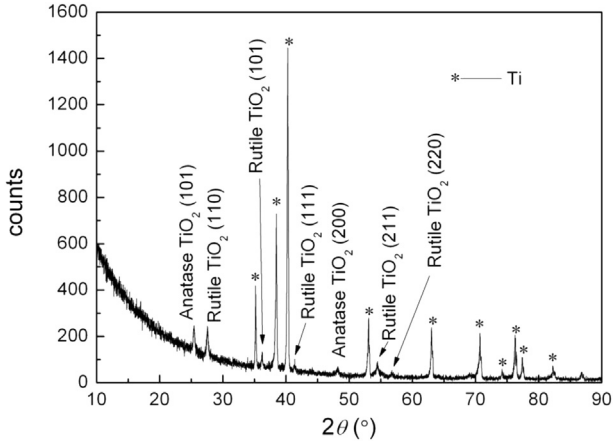

Fig. 4. XRD pattern of RTT electrodes.

The discharge/charge curves of the Li–O_2 batteries at 1.77 A g^{-1} with the RTT as cathodes are presented in Fig. 6. The discharge/charge curves of the batteries with super P using a current density of 1 A g^{-1} are shown in Fig. S1. Obviously, the battery exhibits a much lower capacity (220 mAh g^{-1}) than that with RTT cathode, despite using a lower discharge/charge current density on the former battery. Furthermore, the battery with super P behaves larger overpotentials both in discharge and charge processes (2.3 V and 3.9 V, respectively) compared with RTT catalyzed battery on a 1.77 A g^{-1} current density (Fig. 6), although the former battery is operated with a lower current density. By the way, the battery with super P even cannot run to release any capacity under the current density of 1.77 A g^{-1} in our experiments. The XPS results of the discharged RTT cathodes demonstrate that, the discharge product is Li_2O_2, as seen in Fig. 7, consistent with that of carbon based cathodes [26,27]. Fig. 7 shows the Li 1s XPS pattern of the cathodes after

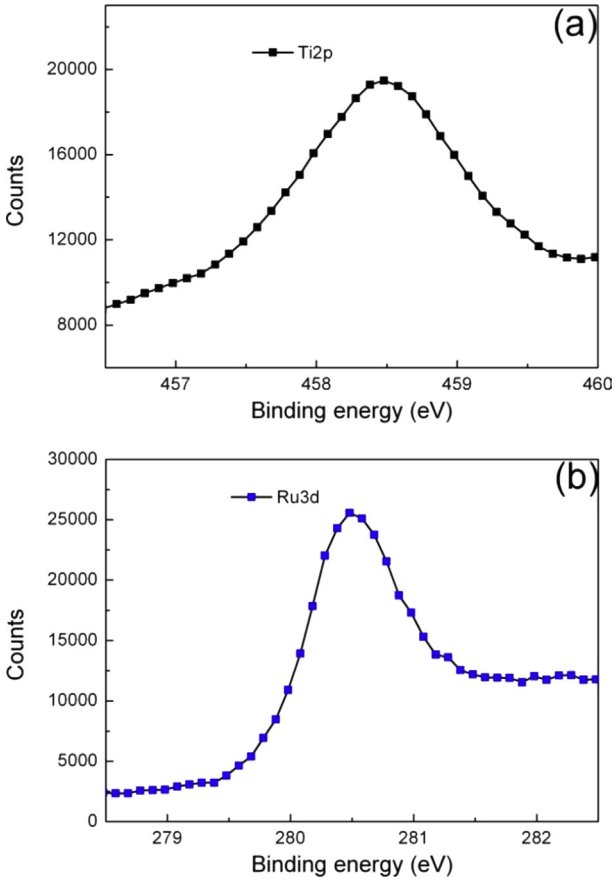

Fig. 5. High resolution XPS patterns of Ti 2p and Ru 3d on the RTT electrodes.

discharge, from which it can be concluded that lithium oxides appear to be formed as the dominant discharge product of the electrochemical reactions. Based on the previous results on the discharged sample using the same electrolyte, [28] the peak (55.5 eV for Li 1s) can be assigned to Li_2O_2. Unfortunately, the batteries with RTT exhibit unsatisfying rate performances that, the overpotentials increase sharply as the discharge/charge current rising to 3.5 A g^{-1}, as seen in Fig. 6. We suggest the unfavorable overpotentials at higher current resulting from the poor supply

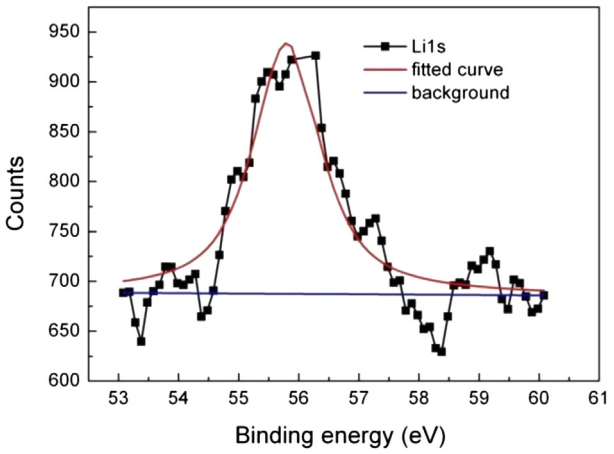

Fig. 7. High resolution XPS pattern of Li 1s on the RTT cathodes after discharge.

capability of oxygen. However, the outstanding stability of TiO_2 and the good catalytic activity of RuO_2 to OER enable the batteries exhibiting excellent reachargeability and cycle performances at the current of 1.77 A g^{-1}. The battery cycles 130 times with the current density of 1.77 A g^{-1} under 1000 mAh g^{-1} capacity limitation, as seen in Fig. 8. The 1st, 50th and 100th discharge/charge curves and the time dependent discharge/charge curves of the Li–O_2 batteries are shown in Fig. S2 and 3. The XRD pattern of the RTT after discharge/charge test has been shown in Fig. S4. The presence of TiO_2 peaks reveals that, TiO_2 can maintain stable in the operation conditions of Li–O_2 batteries. The stability of TiO_2 in Li–O_2 batteries has been also reported in the literatures [20,25]. These results all demonstrate the batteries behaving superior cyclability. We suggest that, the superior cycle performances result from the good catalyzing OER ability and the facilitated oxygen transport channel. Although the discharge voltage fades with the cycle number obviously, the charge voltage still maintains around 3.7 V, as seen in Fig. 9. The outstanding catalytic ability of RuO_2 to the OER lets the precipitate of discharge product decomposing well in the charge processes, which leads the catalyst surface reproducible in the whole cycle test. Otherwise, the interspace with micrometers in the Ti foams and the macropores with one hundred nanometers in the TiO_2 nanotubes combine to form facilitated oxygen transport channels in the RTT cathodes, which guarantee the discharge/charge processes harming by the oxygen diffusion polarization in a

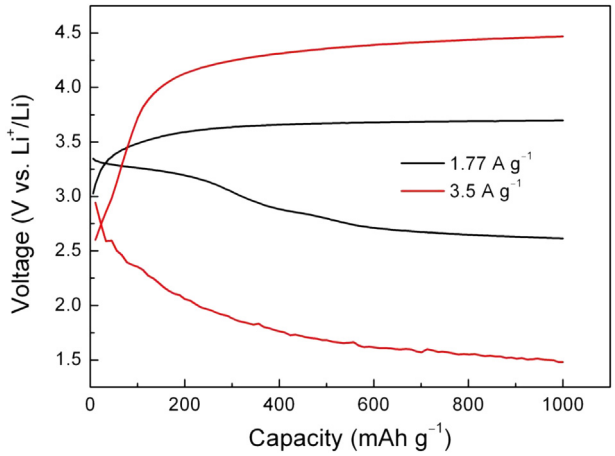

Fig. 6. Discharge/charge curves of the Li–O_2 batteries with RTT at the current density of 1.77 and 3.5 A g^{-1} with the capacity limitation of 1000 mAh g^{-1}.

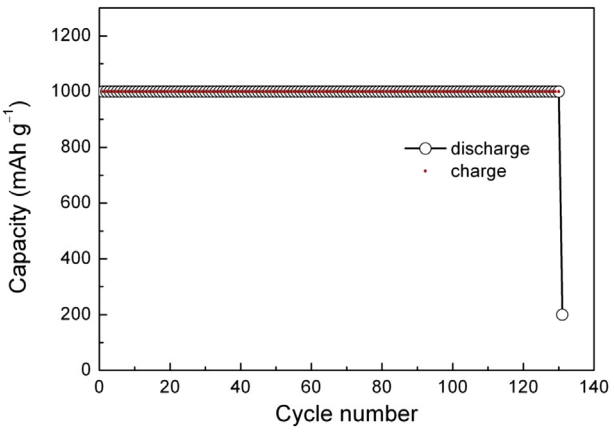

Fig. 8. Cycle performance of the Li–O_2 batteries with RTT at the current density of 1.77 A g^{-1} and the capacity limitation of 1000 mAh g^{-1}.

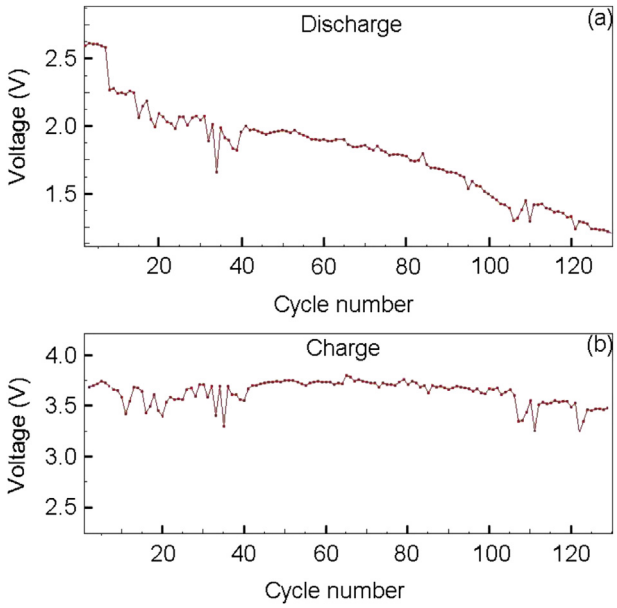

Fig. 9. The discharge and charge end voltage depending on cycle number of the Li–O_2 batteries with RTT at the current density of 1.77 A g^{-1} and the capacity limitation of 1000 mAh g^{-1}.

minimum. These two characteristics endow the cathodes excellent performances in the charge processes by two improvements, the speed of electrode reaction and mass transport.

4. Conclusion

To avoid harming from the decomposition of carbon materials and organic binders, the TiO_2 nanotube arrays coated Ti foams are used as the cathode catalyst support for Li–O_2 batteries in present study. The stability of Ti metal and TiO_2 in the Li–O_2 battery operation conditions guarantees the cathodes having not decomposition and other side reactions, which are the prime negative factors harming the batteries' rechargeability. On the other hand, the macropores in the Ti foams and the straight channel in the TiO_2 nanotubes supply the cathodes facilitated oxygen transport path in the discharge/charge processes. This porous architecture can improve the rechargeability of Li–O_2 batteries, by leading oxygen diffusing to/out of the catalyst easily. RuO_2 catalyst is deposited on the support by an electrodeposition assistant method, forming a carbon and binder free cathode for Li–O_2 batteries. The battery test results reveal that, RuO_2 has good catalytic activity toward OER, which leads the charge voltage retaining around 3.7 V after hundred cycles. The favorable OER catalytic ability and the facilitated oxygen transport channels of the RTT cathodes enable the batteries exhibiting excellent cycle performances.

Acknowledgments

This work was supported by the National Science Foundation of China (NSFC) (No. 21203044) and Fundamental Research Funds for the Central Universities (No. HIT. IBRSEM. A. 201407).

Appendix A. Supplementary data

Supplementary data related to this article can be found at http://dx.doi.org/10.1016/j.jpowsour.2014.07.112.

References

[1] H.-G. Jung, Y.S. Jeong, J.-B. Park, Y.-K. Sun, B. Scrosati, Y.J. Lee, ACS Nano 4 (2013) 3532–3539.
[2] B. Sun, P. Munroe, G. Wang, Sci. Rep. 3 (2013) 2247–2253.
[3] Z. Jian, P. Liu, F. Li, P. He, X. Guo, M. Chen, H. Zhou, Angew. Chem. Int. Ed. 53 (2014) 442–446.
[4] E. Yilmaz, C. Yogi, K. Yamanaka, T. Ohta, H.R. Byon, Nano Lett. 13 (2013) 4679–4684.
[5] M.M.O. Thotiyl, S.A. Freunberger, Z. Peng, P.G. Bruce, J. Am. Chem. Soc. 135 (2013) 494–500.
[6] Z. Peng, S.A. Freunberger, Y. Chen, P.G. Bruce, Science 337 (2012) 563–566.
[7] D.M. Itkis, D.A. Semenenko, E.Yu Kataev, A.I. Belova, V.S. Neudachina, A.P. Sirotina, M. Hävecker, D. Teschner, A. Knop-Gericke, P. Dudin, A. Barinov, E.A. Goodilin, S.-H. Yang, L.V. Yashina, Nano Lett. 13 (2013) 4697–4701.
[8] R. Younesi, M. Hahlin, M. Treskow, J. Scheers, P. Johansson, K. Edström, J. Phys. Chem. C 116 (2012) 18597–18604.
[9] W. Xu, V.V. Viswanathan, D.Y. Wang, S.A. Towne, J. Xiao, Z.M. Nie, D.H. Hu, J.G. Zhang, J. Power Sources 196 (2011) 3894–3899.
[10] R. Black, S.H. Oh, J.H. Lee, T. Yim, B. Adams, L.F. Nazar, J. Am. Chem. Soc. 134 (2012) 2902–2905.
[11] E. Nasybulin, W. Xu, M.H. Engelhard, Z. Nie, X.S. Li, J.-G. Zhang, J. Power Sources 243 (2013) 899–907.
[12] A. Riaz, K.-N. Jung, W. Chang, S.-B. Lee, T.-H. Lim, S.-J. Park, R.-H. Song, S. Yoon, K.-H. Shin, J.-W. Lee, Chem. Commun. 49 (2013) 5984–5986.
[13] F. Li, D.-M. Tang, Y. Chen, D. Golberg, H. Kitaura, T. Zhang, A. Yamada, H. Zhou, Nano Lett. 13 (2013) 4702–4707.
[14] X. Hu, X. Han, Y. Hu, F. Cheng, J. Chen, Nanoscale 6 (2014) 3522–3525.
[15] H. Zhou, L. Liu, K. Yin, S.L. Liu, G.X. Li, Electrochem. Commun. 8 (2006) 1168–1172.
[16] X.W. Li, G.C. Wang, X.X. Li, D.M. Lu, Appl. Surf. Sci. 229 (2004) 395–401.
[17] Q.T. Vu, M. Pavlik, N. Hebestreit, U. Rammelt, W. Plieth, J. Pfleger, React. Funct. Polym. 65 (2005) 69–77.
[18] J.C. Xu, W.M. Liu, H.L. Li, Mater. Sci. Eng. C 25 (2005) 444–447.
[19] A. Dey, S. De, A. De, S.K. De, Nanotechnology 15 (2004) 1277–1283.
[20] M.M.O. Thotiyl, S.A. Freunberger, Z. Peng, Y. Chen, Z. Liu, P.G. Bruce, Nat. Mater. 12 (2013) 1050–1056.
[21] M. Tian, G. Wu, A. Chen, ACS Catal. 2 (2012) 425–432.
[22] G. Zhao, Z. Xu, K. Sun, J. Mater. Chem. A 1 (2013) 12862–12867.
[23] C.C. Hu, K.H. Chang, M.C. Lin, Y.T. Wu, Nano Lett. 6 (2006) 2690–2695.
[24] C.C. Hu, Y.H. Huang, J. Electrochem. Soc. 146 (1999) 2465–2471.
[25] G. Zhao, R. Mo, B. Wang, L. Zhang, Kening Sun, Chem. Mater. 26 (2014) 2551–2556.
[26] H.-D. Lim, K.-Y. Park, H. Song, E.Y. Jang, H. Gwon, J. Kim, Y.H. Kim, M.D. Lima, R.O. Robles, X.L. Ray, H. Baughman, K. Kang, Adv. Mater. 25 (2013) 1348–1352.
[27] H.-G. Jung, J. Hassoun, J.-B. Park, Y.-K. Sun, B. Scrosati, Nat. Chem. 4 (2012) 579–585.
[28] Y. Qin, J. Lu, P. Du, Z. Chen, Y. Ren, T. Wu, J.T. Miller, J. Wen, D.J. Miller, Z. Zhang, K. Amine, Energy Environ. Sci. 6 (2013) 519–531.